Progress In Electromagnetics Research B, Vol. 18, 327–346, 2009

DESIGN OF A BEAM FORMING DIELECTRIC CYLINDRICAL EBG ANTENNA

C. Biancotto and P. Record

School of Engineering & Physical Sciences
Heriot-Watt University
Edinburgh, UK

Abstract—A novel dielectric cylindrical electronic bandgap antenna is presented and analysed using an in-house developed Finite-Difference-Time-Domain software simulator. The design steps and the simulations results of a geometrical parametric study are also presented and discussed, focusing on the design of antennas to operate in the X-band with high directivity patterns on the H-plane. Finally, the measurements results of a set of experiments carried out on a prototype showed very good agreement with simulations: 11% fractional bandwidth at 10 GHz and an average gain of 9.5 dBi are achieved in the impedance bandwidth with 13 dB front-to-back-ratio in the azimuthal plane.

1. INTRODUCTION

Electromagnetic BandGap (EBG) structures [1, 2] and their characteristics have found numerous applications in antenna design. An EBG structure can be realized arranging metallic or dielectric elements in a periodic lattice; the lattice geometry influences the presence, position and extension of frequency bands in which electromagnetic propagation is forbidden (bandgaps). Breaking the periodicity allows electromagnetic energy to propagate through the defect.

Several EBG structures have been presented in literature. Planar woodpile dielectric structures placed over a ground plane have been used by Weily et al. to create a resonator antenna which directivity is proportional to the area of the woodpile aperture [3, 4]; Lee et al. used a similar structure for millimetre-waves which side-lobes where reduced by tapering the woodpile structure periodicity [5, 6]. In both cases the high realized gains in the normal direction can be attributed to the

Corresponding author: C. Biancotto (cb91@hw.ac.uk).

electric field distribution between dielectric superstrate and ground plane: at bandgap frequencies the standing wave type distribution synthesizes an aperture larger than the enclosed antenna.

Defects in the EBG structure can be used to direct the flow of electromagnetic energy [7–9] or to create resonating structures at frequencies within the bandgap [9, 10]. In [7] a sectoral horn antenna based on the electromagnetic confinement mechanism of a woodpile dielectric structure has been presented. The horn antenna side walls are created by flaring apart the rods of one specific layer and it is fed by a defect waveguide created by removing a single rod from the woodpile structure; the achieved bandwidth is within the structure bandgap frequencies with the typical sectoral horn radiation patterns. The concept has been extended in [8] to create a linear array of woodpile EBG sectoral horn antennas. Ozbay et al. [9, 10] presented a monopole antenna surrounded by planar woodpile structure in which a planar defect was formed by separating 2 layers within the structure. The planar defect and the asymmetric positioning of the enclosed monopole achieved a very directional beam in both planes.

Cylindrical EBG (CEBG) structures have been also used in antenna design. CEBG structures made with metallic patches surrounding a dipole antenna [11] or a cylindrical patch antenna [12] have been studied by Palikiras et al: these structures act as partially reflective surfaces and enhance the E-plane directivity pattern of the enclosed antenna. Metallic rods have been used by Chreim et al. to design CEBG antenna structures which achieved omnidirectional [13, 14] and multibeam azimuthal patterns [15]. Boutayeb et al. [16, 17] presented antennas in which a metallic rods CEBG structure with an angular defect window improved the directivity of the enclosed monopole feed.

Dielectric CEBG structures have been also presented in literature: Lee et al. [6, 18] achieved directivity on the E-plane using cylindrical woodpile structures. In [19] the authors presented the simulation results of a novel dielectric CEBG antenna realized with dielectric rods arranged in a simple multilayer cylindrical geometry similar to the one proposed in [16, 17], showing that the aforementioned geometry can also be used to create dielectric CEBG structures. Beam forming and high directivity on the azimuthal plane were achieved by breaking the CEBG structure cylindrical periodicity with an angular defect window: radiation is allowed in the defect direction and forbidden in the opposite directions by the existing bandgap.

In this paper we present the simulations and measurements results of a parametrical study carried out on the CEBG antenna structure presented in [19]. The aim of this study is to analyse the relationships

between geometrical parameters and antenna performances.

A similar approach to [17, 19] has been used: an in-house developed Finite-Difference-Time-Domain (FDTD) simulator has been used to characterize 2D CEBG structures in terms of transmission coefficient and bandgap frequencies; these information have been used to design a 3D CEBG structure; the 3D CEBG structure has been parametrically studied with FDTD simulations and measurements carried out on prototypes built using cylindrical ceramic rods with dielectric constant equals to 76.5. Finally, measurements and simulations results were compared and analysed.

2. CYLINDRICAL EBG STRUCTURE

The 2D CEBG structure, Figure 1(a), is composed by infinite long dielectric rods disposed in a simple multilayer cylindrical geometry. Layers are periodically spaced by P_r, the radial period, whilst dielectric rods are periodically spaced on each layer by P_t, the transverse period. The n-th layer radius and number of rods are respectively equal to $n \cdot P_r$ and $n \cdot N_1$, where N_1 is the first layer number of rods.

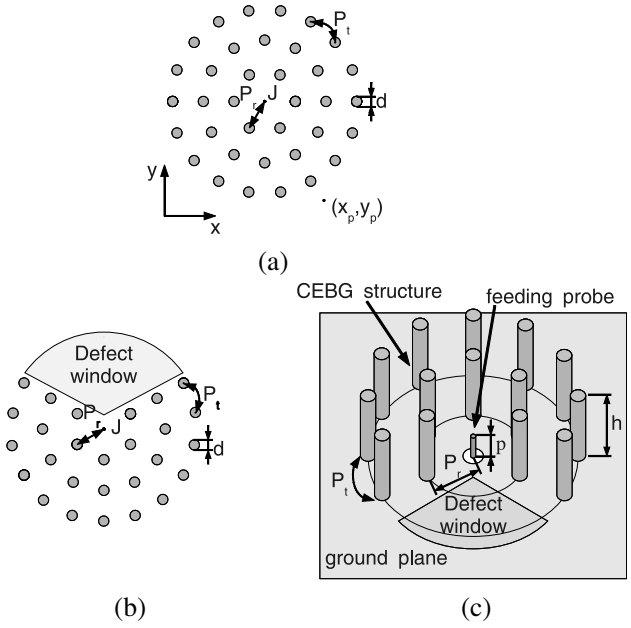

Figure 1. (a) 2D Cylindrical EBG structure; (b) 2D CEBG antenna; (c) 3D CEBG antenna.

Transverse period P_t, radial period P_r and first layer number of rods N_1 are related by:

$$P_t = \frac{2\pi n P_r}{n N_1} = \frac{2\pi P_r}{N_1} \tag{1}$$

where n represents the n-th layer.

The structure is fed by an infinite long current line source (J) placed in the axis which excites a TM cylindrical wave.

The characterization of this structure is based on the transmission coefficient T, extracted by normalizing the transverse electric field $E(x_p, y_p)|_{\mathrm{CEBG}}$ recorded when the CEBG structure is present with the transverse electric field $E(x_p, y_p)|_0$ recorded when the CEBG structure is not present:

$$T = \frac{E(x_p, y_p)|_{\mathrm{CEBG}}}{E(x_p, y_p)|_0} \tag{2}$$

Bandgap position and extension are functions of the above mentioned geometrical parameters, rods dielectric constant ε_r and diameter d.

Figure 2(a) shows the transmission coefficient T as a function of frequency and number of layers for a CEBG structure with $N_1 = 6$, $P_r = 15\,\mathrm{mm}$, $d = 5\,\mathrm{mm}$ and $\varepsilon_r = 76.5$; there are 3 bandgaps in

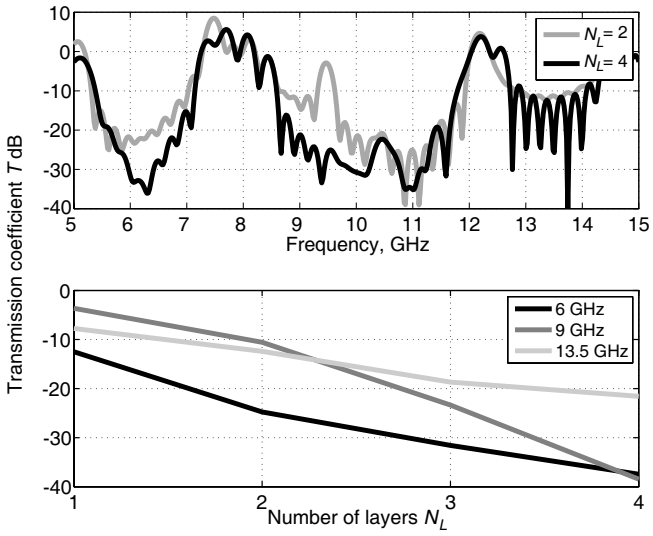

Figure 2. Transmission coefficient T of a CEBG structure with $N_1 = 6$, $P_r = 15\,\mathrm{mm}$, $d = 5\,\mathrm{mm}$ and $\varepsilon_r = 76.5$: above, as a function of frequency; below, as a function of number of layers N_L.

this structure in the shown frequency range: 5.2–7.2 GHz, 8.5–12 GHz and 12.7–14.3 GHz. As shown in Figure 2(b) T, expressed in dB, decreases linearly inside the bandgaps with the number of layers. This suggests that, within the bandgaps, the electric field is evanescent and decaying exponentially while propagating through the CEBG structure as expected [2].

Once the first layer number of rods and dielectric material were chosen, a 4 layer structure was parametrically studied and the results can be visualized in bandgaps as the ones shown in Figure 3. The stopband is set at $T = -10$ dB. These gapmaps are convenient tools to visualize bandgap behaviour as a function of the geometrical parameters; from Figures 3(a) and 3(b) we can see that $d = 5$ mm and $P_r = 15$ mm present a bandgap which almost covers the whole X-band (dashed lines).

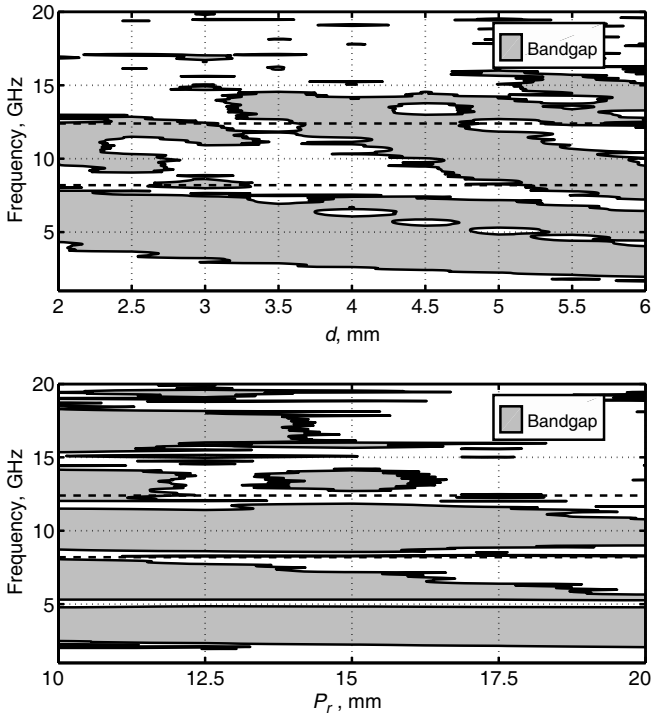

Figure 3. Gapmaps of a CEBG structure with $N_1 = 6$, $\varepsilon_r = 76.5$ and $N_L = 4$: above, as a function of d, $P_r = 15$ mm; below, as a function of P_r, $d = 5$ mm.

3. 2D CEBG ANTENNA

Figure 1(b) depicts a 2D CEBG antenna structure in which directivity is realized by opening an angular defect window in the CEBG structure.

The antenna is designed to operate at frequencies where the full structure presents a bandgap: gain is expected in the same angular direction as the defect whilst in the opposite direction, where the CEBG is intact, the radiation is strongly attenuated. The defect window is created by removing 1 rod from first layer, 3 rods from second layer and so on as shown in Figure 1(b). Other defect window configurations were analysed, as the two depicted in Figure 4 and labeled *win1* and *win2*, but the chosen configuration, *win3*, is very directive for a wider range of frequencies as shown in Figure 5.

Figure 6 show the normalized H-plane radiation pattern of a 2D CEBG antenna with the physical dimensions given in Figure 2. Two layers were found sufficient to achieve high directivity, Figure 6(a); Figure 6(b) also show that directivity is high at 10 GHz, inside the bandgap, but low at frequencies outside the bandgap, 8 GHz and 12.5 GHz.

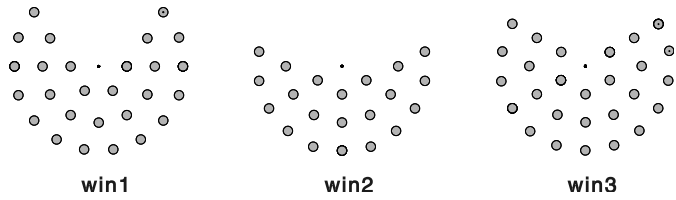

Figure 4. Defect windows geometries.

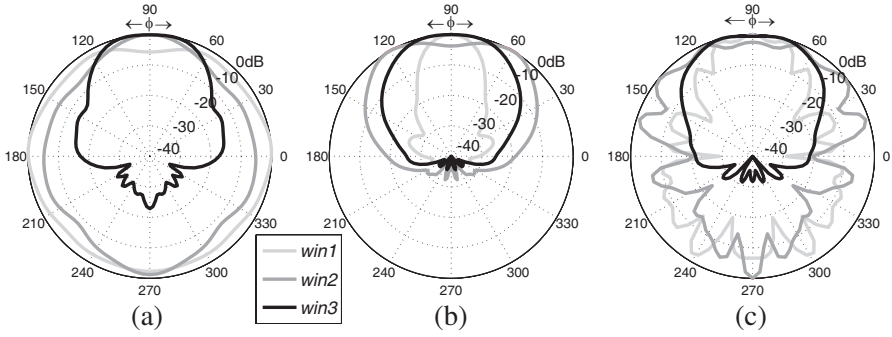

Figure 5. 2D CEBG antenna radiation patterns for the defect windows shown in Figure 4, $N_1 = 6$, $P_r = 15$ mm, $d = 5$ mm, $\varepsilon_r = 76.5$ and $N_L = 4$: (a) 8.5 GHz; (b) 10 GHz; (c) 11.5 GHz.

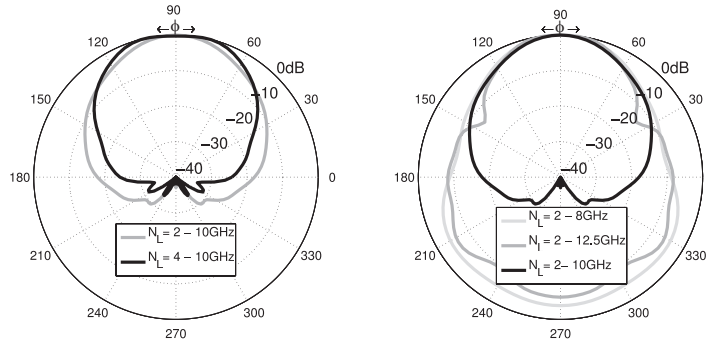

Figure 6. 2D CEBG antenna radiation patterns, $N_1 = 6$, $P_r = 15\,\text{mm}$, $d = 5\,\text{mm}$ and $\varepsilon_r = 76.5$: (a) 10 GHz as a function of layers; (b) $N_L = 2$, as a function of frequency. 2 layers are enough to achieve high directivity at 10 GHz; at frequencies outside the bandgap, 8 GHz and 12.5 GHz, radiation patterns are less directive.

4. 3D CEBG ANTENNA

Using the information gathered from the previous steps, a 3D CEBG antenna, depicted in Figure 1(c), has been designed and simulated with $N_1 = 6$, $P_r = 15\,\text{mm}$, $d = 5\,\text{mm}$, $\varepsilon_r = 76.5$, rods length h and N_L layers; excitation is given through a quarter-wavelength probe of length p which excites TM modes. In all simulations the antenna structure is placed above an infinite ground plane.

The 3D CEBG structure is a finite approximation of an infinite long structure as the ones analysed in the previous sections. For low elevation angles, the excited modes have a strong radially propagating component which is expected to be attenuated by the structure bandgap; for greater angles, although the structure is not expected to attenuate the propagating mode, low radiation is expected given the intrinsic configuration of the excited modes. Thus, as for the 2D case, gain is expected in the same angular direction of the defect window whilst in the opposite direction, where the structure is intact, the radiation is attenuated.

4.1. The Finite-difference Time-domain simulator

The in-house developed simulator is based on the FDTD algorithm implementation in rectangular coordinates [20]; computational space is discretized with spacial steps dx, dy and $dz \geq \lambda/10$ at the frequencies

of interest. A 10 cells thick UPML boundary conditions are used to truncate the computational space [21]. The S_{11} response of the antenna is extracted using a 1D coaxial transmission line coupled to the 3D computational space at the ground plane interface: the monopole feed can be visualized as the coaxial cable inner conductor protruding through the ground plane. Finally, radiation patterns are computed using the near to far fields transformation exposed in [21]: near fields are transformed into far field using a Discrete-Fourier-Transform (DFT) on-the-fly.

4.2. Prototype Simulation and Measurements

A prototype was simulated, built and tested using cylindrical ceramic rods (D_{77} modified barium titanate $\varepsilon_r = 76.5 \pm 2$ [22]) placed on a 150 mm × 150 mm copper ground plane, disposed in a 2 layers 3D CEBG structure with $N_1 = 6$, $P_r = 15$ mm and $d = 5$ mm, $h = 20$ mm and $p = 7.2$ mm. The antenna has been designed to operate in the X-band in order to take advantage of our labs facilities.

In Figures 7–9 simulations and measurements are compared showing a very good agreement; −10 dB bandwidth goes from 9.7 GHz to 10.8 GHz, 11% fractional bandwidth, average gain and front-to-back-ratio of 9.5 dBi and 13 dB respectively within the bandwidth. Best performance are achieved at 9.7 GHz with gain and FTBR equal to 11.5 dBi and 22 dB respectively, Figure 9. The gain decreasing in the measurements for low elevation angle, Figure 8, is caused by the finite ground plane used for the prototype; simulations used an infinite ground plane. Discrepancies between simulations and measurements can be also attributed to tolerances in rods dimensions and position.

Figure 10 shows the electric field distribution on the azimuthal

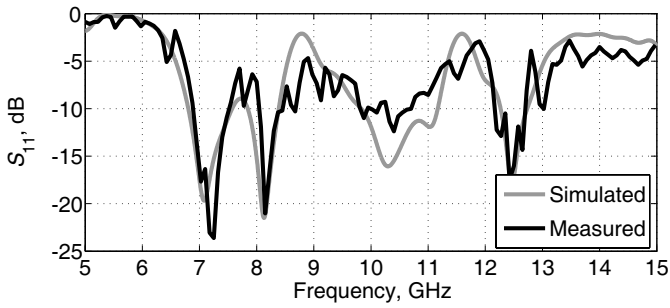

Figure 7. 2 layer 3D CEBG antenna simulated and measured S_{11}; $N_1 = 6$, $P_r = 15$ mm, $d = 5$ mm, $\varepsilon_r = 76.5$ and $h = 20$ mm.

plane at four different frequencies. If we compare this figure with Figure 2(a) it's clear that at bandgap frequencies (6.6 GHz and 10 GHz) the electric field is strongly attenuated by the the CEBG structure; at frequencies outside the bandgap (8 GHz and 12.5 GHz) the electric field is not attenuated by the CEBG structure. This confirms the design assumptions that at low elevation angles the 3D CEBG structure is a good approximation of the 2D CEBG structure. For greater elevation angles the 3D CEBG structure is less effective but it's balanced by the intrinsic nature of the mode excited by the quarter-wavelength probe (the electric field magnitude is decreasing as the elevation angle increases).

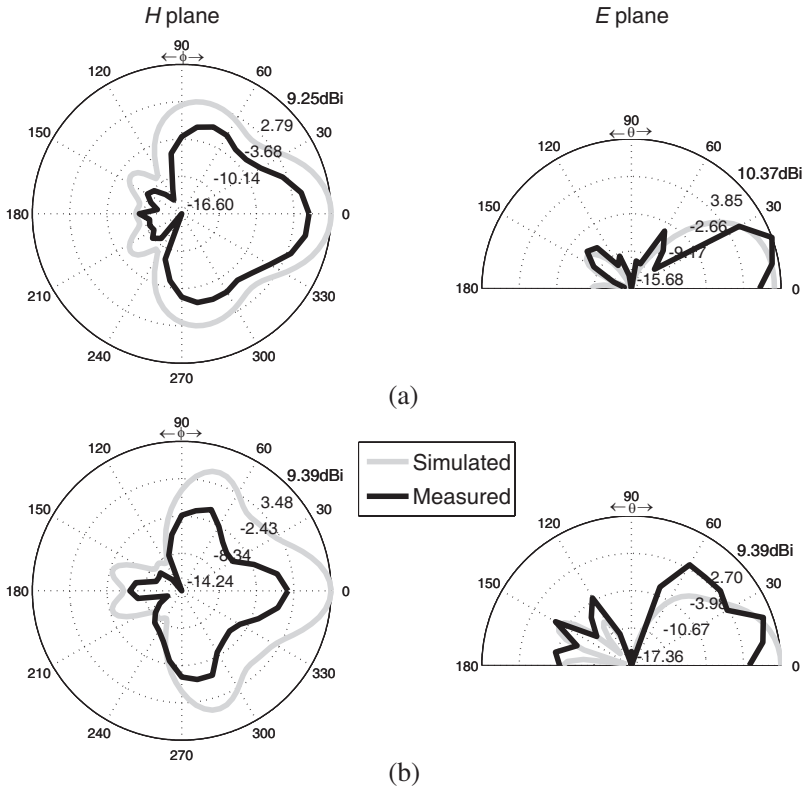

Figure 8. 3D CEBG antenna simulated and measured radiation patterns, $N_1 = 6$, $P_r = 15\,\text{mm}$, $d = 5\,\text{mm}$, $\varepsilon_r = 76.5$ and $h = 20\,\text{mm}$: (a) 9.8 GHz; (b) 10.6 GHz.

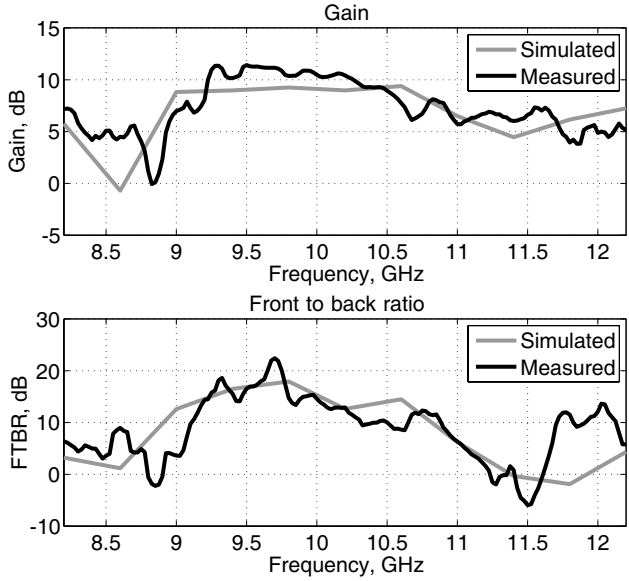

Figure 9. 2 layer 3D CEBG antenna simulated and measured gain (above) and front-to-back-ratio (below); $N_1 = 6$, $P_r = 15\,\text{mm}$, $d = 5\,\text{mm}$, $\varepsilon_r = 76.5$ and $h = 20\,\text{mm}$.

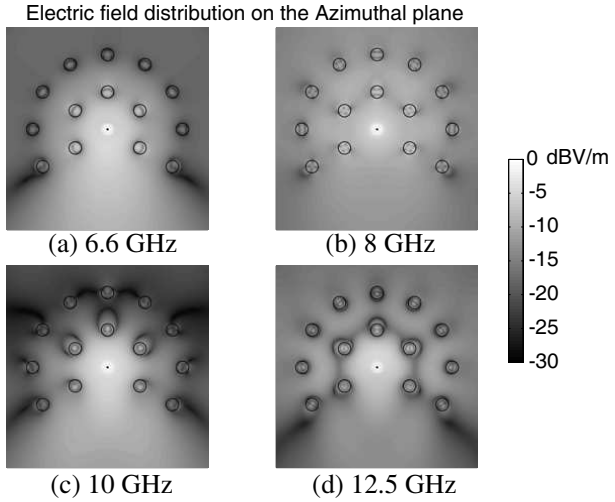

Figure 10. Electric field distribution on the azimuthal plane, $N_1 = 6$, $P_r = 15\,\text{mm}$, $d = 5\,\text{mm}$, $\varepsilon_r = 76.5$ and $h = 20\,\text{mm}$: (a) 6.6 GHz; (b) 8 GHz; (c) 10 GHz; (d) 12.5 GHz.

5. PARAMETRIC STUDY

As reported in Section 2, the geometrical parameters N_1, P_r and d along with ε_r are responsible for bandgaps positions, these parameters are chosen accordingly to antenna frequencies of operation. The remaining two geometrical parameters, h and N_L, have been parametrically studied to analyse their influence on antenna's performance.

5.1. Number of Layers — N_L

Figure 11 shows the antenna S_{11} as a function of N_L ($h = 20\,\text{mm}$). Increasing the number of layers improves the matching within the impedance bandwidth but the overall differences are very small. The S_{11} response also presents several resonances at higher and lower frequencies; it's interesting to note that the for $N_L = 1$ the lower frequency resonances merge to form a second band between 6.8 and 8.5 GHz. Radiation pattern is also influenced by the number of layers; as shown in Figures 12–14 and summarised in Table 1, increasing the number of layers improves antenna gain and directivity patterns. Gain and FTBR are considerably improved when the number of layers N_L is increased from 1 to 2 but differences are minimal when increased from 2 to 3.

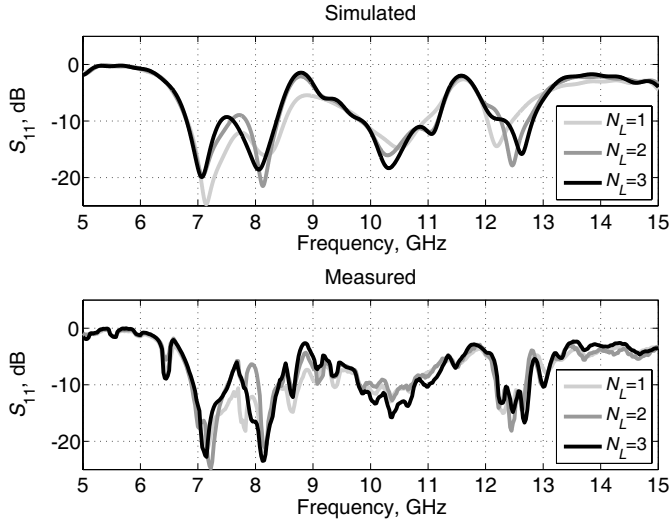

Figure 11. 3D CEBG antenna simulated and measured S_{11} as a function of number of layers N_L; $N_1 = 6$, $P_r = 15\,\text{mm}$, $d = 5\,\text{mm}$, $\varepsilon_r = 76.5$ and $h = 20\,\text{mm}$.

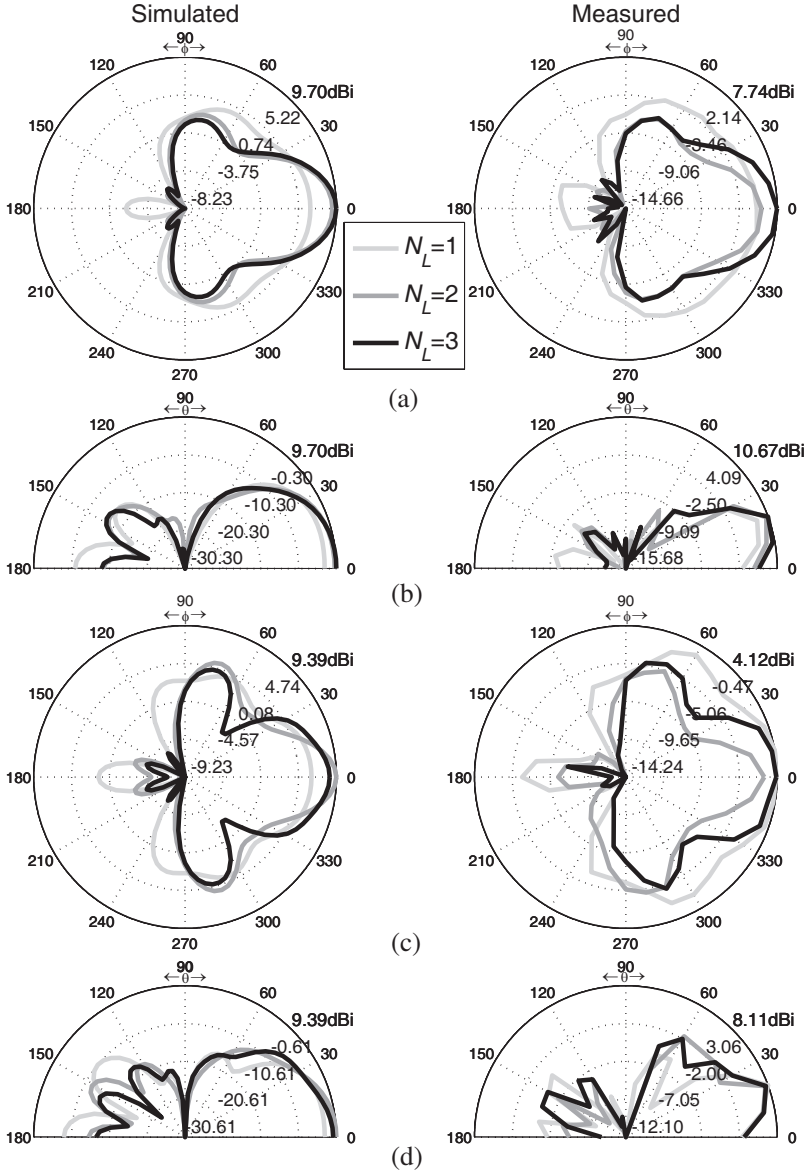

Figure 12. 3D CEBG antenna simulated (left) and measured (right) radiation patterns as a function of number of layers N_L; $N_1 = 6$, $P_r = 15\,\text{mm}$, $d = 5\,\text{mm}$, $\varepsilon_r = 76.5$ and $h = 20\,\text{mm}$: (a) H-plane at 9.8 GHz; (b) E-plane at 9.8 GHz; (c) H-plane at 10.6 GHz; (d) E-plane at 10.6 GHz.

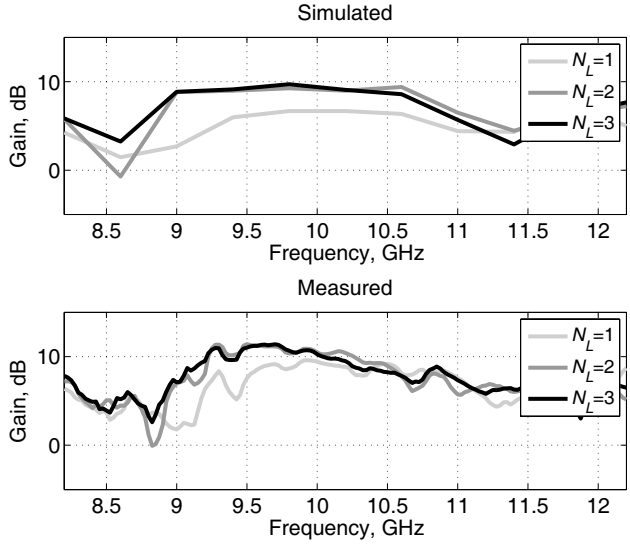

Figure 13. 3D CEBG antenna simulated and measured gain as a function of number of layers N_L; $N_1 = 6$, $P_r = 15\,\text{mm}$, $d = 5\,\text{mm}$, $\varepsilon_r = 76.5$ and $h = 20\,\text{mm}$.

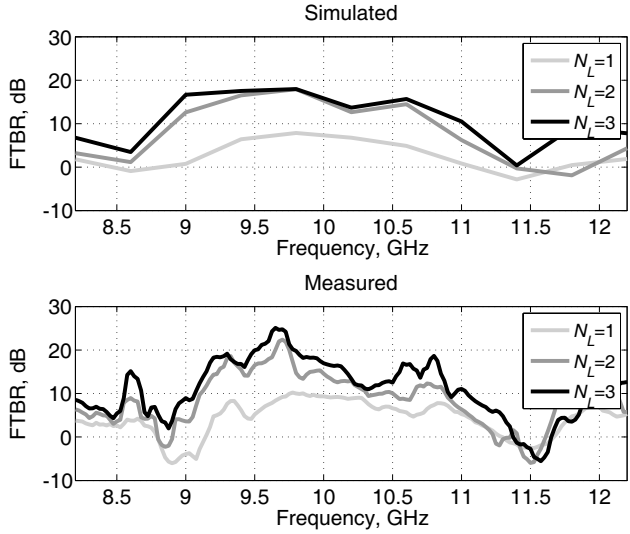

Figure 14. 3D CEBG antenna simulated and measured front-to-back-ratio (FTBR) as a function of number of layers N_L; $N_1 = 6$, $P_r = 15\,\text{mm}$, $d = 5\,\text{mm}$, $\varepsilon_r = 76.5$ and $h = 20\,\text{mm}$.

Table 1. 3D CEBG antenna simulated (in brackets) and measured performance as a function of number of layers N_L; $N_1 = 6$, $P_r = 15\,\text{mm}$, $d = 5\,\text{mm}$, $\varepsilon_r = 76.5$ and $h = 20\,\text{mm}$.

N_L	Gain, dBi	FTBR, dB	BW, %
1	9.6 (7.6)	10.2 (7.8)	11 (10.2)
2	11.4 (9.4)	22.4 (17.9)	11 (12.7)
3	11.4 (9.7)	25.1 (17.9)	11 (12.7)

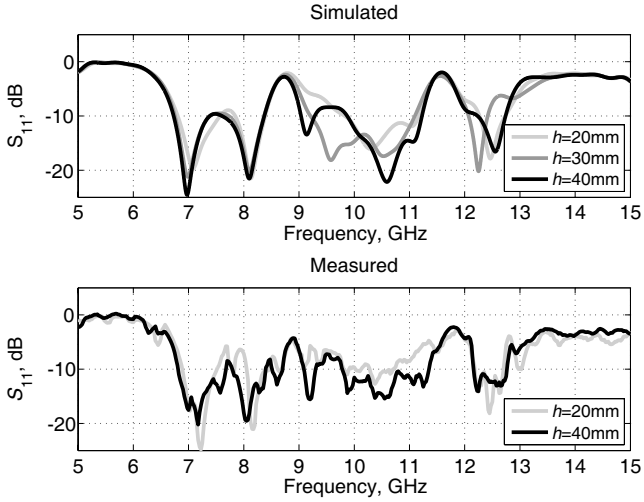

Figure 15. 3D CEBG antenna simulated and measured S_{11} as a function of rods length h; $N_1 = 6$, $P_r = 15\,\text{mm}$, $d = 5\,\text{mm}$, $\varepsilon_r = 76.5$ and $N_L = 2$.

5.2. Rods Length — *h*

The S_{11} of a 2 layer structure as a function of rods length h is show in Figure 15. Rods length can significantly influence the frequency response of the antenna and as in the previous case a second band can appear between 6.8 and 8.5 GHz. Simulations and measurements shown that increasing h generally improves directivity patterns, gain and FTBR, Figures 16–18 and summarised in Table 2. Impedance bandwidth can also be improved by tuning rods height h: simulations shown that with $h = 30\,\text{mm}$ bandwidth is 40% wider compared to $h = 20\,\text{mm}$, Figure 15; measurements were taken with $h = 20\,\text{mm}$ and 40 mm, showing almost a 50% bandwidth increase in the latter case, Figure 15.

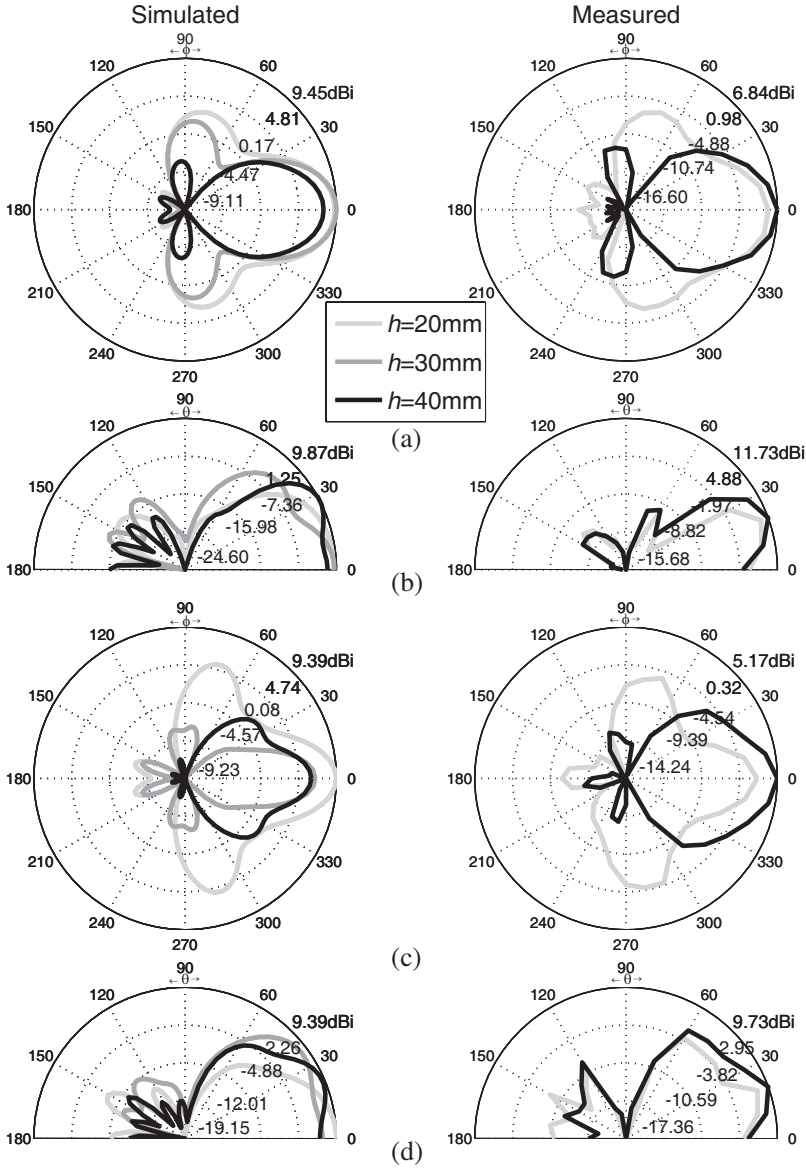

Figure 16. 3D CEBG antenna simulated (left) and measured (right) radiation patterns as a function of rods length h; $N_1 = 6$, $P_r = 15\,\text{mm}$, $d = 5\,\text{mm}$, $\varepsilon_r = 76.5$ and $N_L = 2$: (a) H-plane at 9.8 GHz; (b) E-plane at 9.8 GHz; (c) H-plane at 10.6 GHz; (d) E-plane at 10.6 GHz.

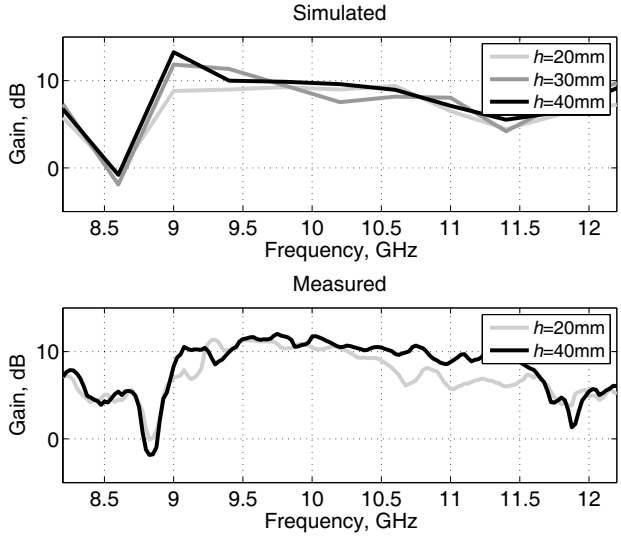

Figure 17. 3D CEBG antenna simulated and measured gain as a function of rods length h; $N_1 = 6$, $P_r = 15\,\text{mm}$, $d = 5\,\text{mm}$, $\varepsilon_r = 76.5$ and $N_L = 2$.

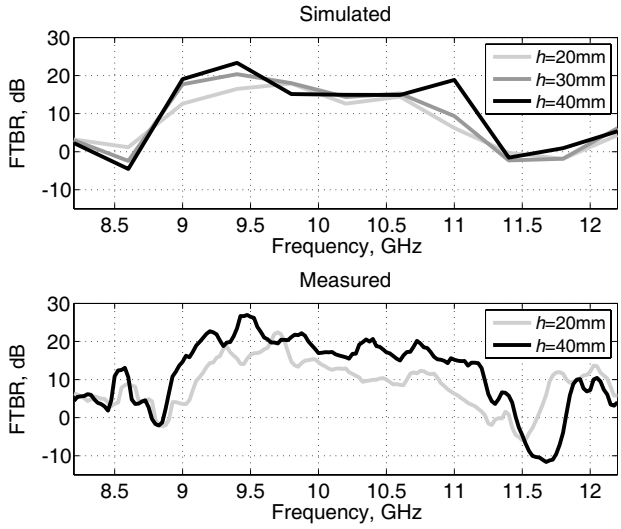

Figure 18. 3D CEBG antenna simulated and measured front-to-back-ratio (FTBR) as a function of rods length h; $N_1 = 6$, $P_r = 15\,\text{mm}$, $d = 5\,\text{mm}$, $\varepsilon_r = 76.5$ and $N_L = 2$.

Table 2. 3D CEBG antenna simulated (in brackets) and measured performance as a function of rods length h; $N_1 = 6$, $P_r = 15\,\text{mm}$, $d = 5\,\text{mm}$, $\varepsilon_r = 76.5$ and $N_L = 2$.

h	Gain, dBi	FTBR, dB	BW, %
20	11.4 (9.4)	22.4 (17.9)	11 (12.7)
30	- (11.8)	- (20.4)	- (18)
40	12 (13.2)	27 (23.3)	16 (13.7)

6. DISCUSSION

The proposed dielectric CEBG (DCEBG) antenna is based on a cylindrical geometry similar to the 4 layer metallic CEBG (MCEBG) antenna presented and analysed in [16, 17]. The presented design approach is similar to the MCEBG antenna design steps, nevertheless the authors have included gapmaps and defect window geometry analysis in the design process: the formers are a convenient tool to visualize the bandgap behaviour as a function of the geometrical parameters in order to optimize their choice; the latter shown which defect window geometry has the best frequency behaviour.

The MCEBG antenna achieved a higher peak gain and a wider fractional impedance bandwidth, respectively 15.8 dBi and 28%, compared to the presented DCEBG antenna, 11.4 dBi peak gain and 11% bandwidth. However, the DCEBG antenna has smaller relative dimensions: 20% narrower diameter (2λ against 2.4λ) and 50% lower profile (0.67λ against 1.33λ). Moreover the required number of rod elements is much lower, 14 dielectric rods are used for the DCEBG antenna and 96 metallic rods for the MCEBG antenna.

The parametric study shown that increasing the number of layers N_L slightly influences antenna's bandwidth but improves radiation patterns and maximum gain, as reported in [17], though the differences between 2 or 3 layers are minimal. This suggests that 2 layers are a good compromise in terms of antenna performances and dimensions for the presented DCEBG antenna.

Rods length h also influence matching and radiation patterns and it can be set in order to optimize gain and bandwidth extension: the 2 layers configuration with $h = 40\,\text{mm}$ achieved 16% fractional bandwidth, 50% wider, and higher peak gain and front-to-back-ratio, respectively 12 dBi and 27 dB.

Although planar EBG structures [3–6, 9, 10], can achieve higher peak gain and narrower beamwidth, the practical operating frequency range for high directivity patterns is usually narrower compared to the

presented DCEBG antenna where the radiation patterns have similar features within the whole impedance bandwidth. In addition to that, the analysed DCEBG antenna has also a simpler geometrical structure and smaller relative dimensions.

7. CONCLUSION

The analysis and the design steps of a novel dielectric CEBG antenna have been presented, showing that this structure can achieve directive patterns on the H-plane. Simulations achieved 16.5% fractional bandwidth, average gain and FTBR of 8 dBi and 15 dB respectively. Measurements were in good agreement with simulations and validated the design approach, achieving a higher gain, 9.5 dBi but a narrower bandwidth, 11% and a slightly lower front-to-back-ratio, 13 dB. Antennas were designed to operate at 10 GHz in order to take advantage of our lab facilities; scaling down or up the geometrical parameters will respectively scale up or down of the same factor the frequency characteristics of the antenna.

A parametric study based on FDTD simulations and prototype measurements has been also presented. The aim of this study was to investigate the relationship between antenna geometrical parameters and performances, focusing on the parameters which are not bound during the design process by bandgap position and frequency of operation, i.e., rods height h and number of layers N_L.

Future work will be focused on the design and testing of antennas realised using similar configurations and different dielectric materials.

REFERENCES

1. Yablonovitch, E., "Inhibited spontaneous emission in solid-state physics and electronics," *Physical Review Letters*, Vol. 58, 2059, May 1987.
2. Joannopoulos, J. D., R. D. Meade, and J. N. Winn, *Photonic Crystals: Molding the Flow of Light*, Appendix D, Princeton, 1995.
3. Weily, A., L. Horvath, K. Esselle, B. Sanders, and T. Bird, "A planar resonator antenna based on a woodpile EBG material," *IEEE Transactions on Antennas and Propagation*, Vol. 53, 216–223, 2005.
4. Weily, A., K. Esselle, B. Sanders, and T. Bird, "Woodpile EBG resonator antenna with double slot feed," *IEEE Antennas and*

Propagation Society International Symposium, Vol. 2, 1139–1142, 2004.

5. Lee, Y., X. Lu, Y. Hao, S. Yang, R. Ubic, J. Evans, and C. Parini, "Directive millimetre-wave antenna based on freeformed woodpile EBG structure," *Electronics Letters*, Vol. 43, 195–196, 2007.
6. Lee, Y., X. Lu, Y. Hao, S. Yang, J. Evans, and C. Parini, "Directive millimetrewave antennas using freeformed ceramic metamaterials in planar and cylindrical forms," *IEEE Antennas and Propagation Society International Symposium*, 1–4, 2008.
7. Weily, A., K. Esselle, B. Sanders, and T. Bird, "A woodpile EBG sectoral horn antenna," *IEEE Antennas and Propagation Society International Symposium*, Vol. 4B, 323–326, 2005.
8. Weily, A., K. Esselle, T. Bird, and B. Sanders, "Linear array of woodpile EBG sectoral horn antennas," *IEEE Transactions on Antennas and Propagation*, Vol. 54, 2263–2274, 2006.
9. Ozbay, E., B. Temelkuran, and M. Bayindir, "Microwave applications of photonic crystals," *Progress In Electromagnetics Research*, PIER 41, 185–209, 2003.
10. Temelkuran, B., M. Bayindir, E. Ozbay, R. Biswas, M. M. Sigalas, G. Tuttle, and K. M. Ho, "Photonic crystal-based resonant antenna with a very high directivity," *Journal of Applied Physics*, Vol. 87, 603–605, Jan. 2000.
11. Palikaras, G., A. Feresidis, and J. Vardaxoglou, "Cylindrical electromagnetic bandgap structures for directive base station antennas," *IEEE Antennas and Wireless Propagation Letters*, Vol. 3, 87–89, 2004.
12. Palikaras, G., A. Feresidis, and Y. Vardaxoglou, "Design of cylindrical omni-directional patch antenna with superimposed EBG surfaces," *Antennas and Propagation Conference LAPC 2007*, Loughborough, 297–300, 2007.
13. Chreim, H., E. Pointereau, B. Jecko, and P. Dufrane, "Omnidirectional Electromagnetic band gap antenna for base station applications," *Antennas and Wireless Propagation Letters*, Vol. 6, 499–502, 2007.
14. Pointereau, E., H. Chreim, B. Jecko, and P. Dufrane, "Omnidirectional cylindrical electromagnetic bandgap antenna with dual polarization," *IEEE Antennas and Wireless Propagation Letters*, Vol. 6, 450–453, 2007.
15. Chreim, H., M. Hajj, E. Arnaud, B. Jecko, C. Dall'omo, and P. Dufrane, "Multibeam antenna for telecommunications networks using cylindrical EBG structure," *IEEE Antennas and Wireless*

Propagation Letters, Vol. 8, 665–669 2009.

16. Boutayeb, H., T. Denidni, A. Sebak, and L. Talbi, "Metallic EBG structures for directive antennas using rectangular, cylindrical and elliptical shapes," *IEEE Antennas and Propagation Society International Symposium 2005*, Vol. 1A, 762–765, 2005.
17. Boutayeb, H., T. Denidni, K. Mahdjoubi, A. Tarot, A. Sebak, and L. Talbi, "Analysis and design of a cylindrical EBG-based directive antenna," *IEEE Transactions on Antennas and Propagation*, Vol. 54, 211–219, 2006.
18. Lee, Y., X. Lu, Y. Hao, S. Yang, C. Parini, and J. Evans, "Cylindrical EBG antenna for short range gigabit wireless communications at millimetre-wave bands," *Electronics Letters*, Vol. 45, 136–138, 2009.
19. Biancotto, C. and P. Record, "Beam forming dielectric cylindrical EBG antenna," *Antennas and Propagation Conference LAPC 2009*, Loughborough, 2009, to be published.
20. Yee, K., "Numerical solution of inital boundary value problems involving maxwell's equations in isotropic media," *Antennas and Propagation, IEEE Transactions on [Legacy, Pre-1988]*, Vol. 14, 302–307, May 1966.
21. Taflove, A., *Advances in Computational Electromagnetics — The Finite-Difference Time-Domain Method*, Artech House, 1998.
22. http://www.morganelectroceramics.com/microwave/D77.htm.